Int J Thermophys (2008) 29:1066–1083
DOI 10.1007/s10765-008-0385-1

Uncertainty Budgets for Calibration of Radiation Thermometers below the Silver Point

P. Saunders · J. Fischer · M. Sadli · M. Battuello · C. W. Park · Z. Yuan · H. Yoon · W. Li · E. van der Ham · F. Sakuma · J. Ishii · M. Ballico · G. Machin · N. Fox · J. Hollandt · M. Matveyev · P. Bloembergen · S. Ugur

Published online: 29 February 2008

Abstract Below the freezing point of silver, radiation thermometers are generally calibrated by implementing the multi-point interpolation method using blackbody measurements at three or more calibration points, rather than the ITS-90 extrapolation technique. The interpolation method eliminates the need to measure the spectral responsivity and provides greater accuracy at the longer wavelengths required below the silver point. This article identifies all the sources of uncertainty associated with the interpolation method, in particular, those related to the reference blackbody temperatures (either variable-temperature or fixed-point blackbodies) and to the measured thermometer signals at these points. Estimates are given of the 'normal' and 'best' uncertainties currently achievable. A model of the thermometer response is used to propagate all the uncertainties at the reference points and provide a total uncertainty

P. Saunders (✉)
Measurement Standards Laboratory of New Zealand (MSL), Industrial Research Ltd,
P.O. Box 31-310, Lower Hutt, New Zealand
e-mail: p.saunders@irl.cri.nz

J. Fischer · J. Hollandt
Physikalisch-Technische Bundesanstalt (PTB), Braunschweig, Germany

M. Sadli
Conservatoire national des arts et métiers/Institut National de Métrologie (LNE-INM/CNAM),
La Plaine-Saint-Denis, France

M. Battuello
Istituto Nazionale di Ricerca Metrologica (INRiM), Turin, Italy

C. W. Park
Korea Research Institute of Standards and Science (KRISS), Daejeon, South Korea

Z. Yuan
National Institute of Metrology (NIM), Beijing, China

H. Yoon
National Institute of Standards and Technology (NIST), Gaithersburg, MD, USA

at any temperature within the calibration range. The multi-point method has the effect of constraining the total uncertainty over this range, unlike the ITS-90 technique for which the uncertainties propagate as T^2. This article is a joint effort of the working group on radiation thermometry of the Consultative Committee for Thermometry (CCT), summarizing the knowledge and experience of all experts in this field.

Keywords Calibration · Radiation thermometry · Uncertainty

1 Introduction

The calibration of radiation thermometers over the temperature range from −50 to 961.78°C (the freezing point of silver) is important for the support of many applications of radiation thermometry, particularly in industry. While the ITS-90 technique for realizing temperature above the silver point may, in principle, also be applied below the silver point, difficulties associated with direct measurement of the thermometer's relative spectral responsivity at the longer wavelengths required often preclude its use. Instead, because of the availability of multiple fixed points and contact thermometers that can measure the temperature of blackbodies according to ITS-90, interpolation methods are used to calibrate radiation thermometers below the silver point.

The relationship between thermometer signal, $S(T)$, and blackbody temperature, T, is

$$S(T) = \int_0^\infty R(\lambda) L_b(\lambda, T) d\lambda, \tag{1}$$

where $R(\lambda)$ is the thermometer's absolute spectral responsivity and $L_b(\lambda, T)$ is Planck's law. Interpolation methods approximate this integral equation with a

W. Li
Standards, Productivity and Innovation Board (NMC/SPRING), Singapore, Singapore

E. van der Ham
Nederlands Meetinstituut/Van Swinden Laboratorium B.V. (NMi/VSL), Delft, The Netherlands

F. Sakuma · J. Ishii · P. Bloembergen
National Metrology Institute of Japan, AIST (NMIJ/AIST), Tsukuba, Japan

M. Ballico
National Measurement Institute of Australia (NMIA), Lindfield, Australia

G. Machin · N. Fox
National Physical Laboratory (NPL), Teddington, UK

M. Matveyev
D.I. Mendeleyev Institute for Metrology, Rostekhregulirovaniye of Russia (VNIIM),
St Petersburg, Russia

S. Ugur
TEKNOYAD, Kemal Nehrozoglu Cad. GOSB Technopark, Gebze, Kocaeli, Turkey

calibration equation containing a small number of adjustable parameters that are determined from a set of N measured temperature–signal pairs, (T_i, S_i), where $i=1$ to N. While many different calibration equations have been used [1–3], empirical evidence suggests that the Sakuma–Hattori equation [4] provides the best compromise among accuracy, ease of use, and number of parameters. The Planck version of this equation is

$$S(T) = \frac{C}{\exp\left(\frac{c_2}{AT+B}\right) - 1}, \tag{2}$$

where A, B, and C are the parameters to be determined by calibration and c_2 is the second radiation constant. The Wien approximation to Eq. 2, which is sometimes used, neglects the -1 in the denominator. At least three temperature–signal pairs are required to determine the values of A, B, and C. When $N=3$, Eq. 2 is an interpolation equation that passes exactly through each pair of points, and when $N > 3$, the parameters are determined by least-squares fitting. A particular advantage of the Sakuma–Hattori and other calibration equations is that they allow a radiation thermometer to be calibrated without any knowledge of its spectral responsivity.

The uncertainty in temperatures determined using Eq. 2 arises from uncertainties in the calibration points (T_i, S_i), from the quality of the match of the calibration equation to the actual signal response of the thermometer (i.e., the difference between Eqs. 1 and 2, which is referred to as interpolation error), from drift subsequent to calibration, and from uncertainties associated with the measurement of the signal at the unknown temperature. These latter "in-use" components differ according to whether the thermometer is used as a reference thermometer or a working thermometer. In the reference thermometer case, the in-use components arise during signal measurements of a blackbody when calibrating some other thermometer. In the case of a working thermometer, the in-use components arise from a multitude of environmental effects, the most important of which relate to the emissivity of the surface of interest, reflection errors from surrounding objects, and atmospheric absorption and emission effects. These working thermometer uncertainties are beyond the scope of this article.

In the temperature range below the silver point, many options are available with regard to operating wavelength and temperature range. Specific examples are presented for four different thermometers: 0.9 µm (420–1, 085°C); 1.6 µm (150–962°C); 3.9 µm (20–962°C); and 8–14 µm (−40 to 500°C), sometimes referred to as a 10-µm thermometer. In many of these cases, the wavelength × temperature product is large enough that the Wien approximation introduces significant error, so the uncertainty analysis is performed taking full account of Planck's law.

This article, which is a summary of an uncertainty guide prepared by the radiation thermometry working group of the CCT [5], catalogues each uncertainty component and evaluates how each component propagates into the unknown temperature. Note that the scope is limited to those thermometers whose signal is proportional to the detector photocurrent. This precludes thermometers that read directly in temperature.

2 Propagation of Uncertainty

Recently, the CCT radiation thermometry working group also published a guide [6,7] on uncertainty budgets for realizing ITS-90 by radiation thermometry above the silver point. Much of the information described there for thermometers working at visible wavelengths is of relevance to near-infrared thermometers (0.9 and 1.6-μm) above the indium point. However, the mathematical formalism required for propagation of uncertainty in the interpolation schemes described here is considerably different. In particular, while the uncertainties in the ITS-90 method tend to increase indefinitely with T^2, in the interpolation schemes the multiple calibration points constrain the uncertainties within the calibration range. The sensitivity coefficients are more complex and are functions of all the calibration temperatures.

In this article, two calibration schemes are considered. One of these uses fixed-point blackbodies (FPBB scheme) to obtain the calibration points (T_i, S_i) and the other uses variable-temperature blackbodies with a separate reference thermometer (VTBB scheme). In practice, a calibration may consist of a combination of these two schemes. From an uncertainty analysis perspective, the only difference between these two schemes is the nature and number of the individual uncertainty components that contribute to the total uncertainty. These are listed in Table 1 for the two schemes, where a shaded box indicates that the component must be included. The table is split into those components related to the blackbody and those related to the radiation thermometer under calibration. Each component is treated as *either* an uncertainty in the temperature of the blackbody, $u_x(T_i)$, *or* a relative uncertainty in the signal measured by the radiation thermometer, $u_x(S_i)/S_i$. Note that the subscript i refers to the calibration point and the subscript x to the uncertainty component for that point. In addition to these "calibration uncertainties," there is also an interpolation error component, which is treated as a constant across the calibration range, a component due to drift, which is a function of the source temperature when the thermometer is used at some time after its calibration, and components related to measurement of the signal at the unknown temperature.

Assuming that all the calibration uncertainties are uncorrelated, the combined calibration uncertainty is given by [8]

$$u_c^2(T) = \left[\sum_{i=1}^{N}\left(\frac{\partial S(T)}{\partial T_i}u(T_i)\right)^2 + \sum_{i=1}^{N}\left(\frac{\partial S(T)}{\partial S_i}S_i\frac{u(S_i)}{S_i}\right)^2\right]\left(\frac{\partial S(T)}{\partial T}\right)^{-2}, \quad (3)$$

where $u(T_i)$ and $u(S_i)/S_i$ are the quadrature sums of each of the $u_x(T_i)$ and $u_x(S_i)/S_i$ components at each calibration point, respectively. When $N = 3$ and the Sakuma–Hattori equation is interpolated exactly, Eq. 3 can be written explicitly as [9]

$$u_c^2(T) = \sum_{i=1}^{3}[f_i(T)u(T_i)]^2 + \sum_{i=1}^{3}\left[f_i(T)\frac{\lambda_{T_i}T_i^2}{c_2}\left[1-\exp\left(-c_2/\lambda_{T_i}T_i\right)\right]\frac{u(S_i)}{S_i}\right]^2, \quad (4)$$

Table 1 Uncertainty components for the FPBB and VTBB calibration schemes. The shaded boxes indicate the uncertainty components included under the respective schemes

	Description	Quantity	FPBB Scheme	VTBB Scheme
Blackbody	Calibration temperature	$u_1(T_i)$		
	Impurities	$u_2(T_i)$		
	Plateau identification	$u_3(T_i)$		
	Blackbody emissivity, isothermal	$u_4(S_i)/S_i$		
	Blackbody emissivity, non-isothermal	$u_5(T_i)$		
	Reflected ambient radiation	$u_6(T_i)$		
	Cavity bottom heat exchange	$u_7(T_i)$		
	Convection	$u_8(T_i)$		
	Cavity bottom uniformity	$u_9(T_i)$		
	Ambient conditions	$u_{10}(T_i)$		
Radiation Thermometer	Size-of-source effect	$u_{11}(S_i)/S_i$		
	Non-linearity	$u_{12}(S_i)/S_i$		
	Reference temperature	$u_{13}(T_i)$		
	Ambient temperature	$u_{14}(S_i)/S_i$		
	Atmospheric absorption	$u_{15}(S_i)/S_i$		
	Gain ratios	$u_{16}(S_i)/S_i$		
	Noise	$u_{17}(T_i)$		
Calibration Equation	Interpolation error	u_{18}		
In-Use	Drift	$u_{19}(T)$		
	Unknown temperature	$u_{20}(T)$		

where

$$\lambda_{T_i} = A\left(1 + \frac{B}{AT_i}\right)^2 \tag{5}$$

Table 2 Typical values of the A and B parameters of the Sakuma–Hattori equation, the mean wavelength, λ_0, the bandwidth, and values of the limiting effective wavelength over typical temperature ranges as calculated by Eq. 5

Spectral Responsivity (μm)	A (μm)	B(μm·K)	λ_0 (μm)	Bandwidth (μm)	Temperature range (°C)	λ_T Range (μm)
0.9	0.896	5.91	0.899	0.083	420–1,085	0.914–0.905
1.6	1.58	5.16	1.590	0.105	150–962	1.604–1.588
3.9	3.90	1.80	3.904	0.165	20–962	3.912–3.903
8–14	9.61	151	11.00	6.00	−40–500	10.95–10.00

is the limiting effective wavelength evaluated at temperature T_i, and A and B are the same quantities as those appearing in Eq. 2. Values of A and B for typical radiation thermometers are given in Table 2.

Under the Wien approximation, the exponential term in Eq. 4 can be neglected and the $f_i(T)$ functions are second-order Lagrange polynomials in T:

$$f_i(T) \approx L_i(T) = \frac{\prod_{j=1, j\neq i}^{3} (T - T_j)}{\prod_{j=1, j\neq i}^{3} (T_i - T_j)}, \text{e.g.,} L_1(T) = \frac{(T - T_2)(T - T_3)}{(T_1 - T_2)(T_1 - T_3)}. \quad (6)$$

However, for operating wavelengths of 3.9 μm and longer, Wien's approximation introduces up to 20% error in the uncertainty values. In this case, the $f_i(T)$ functions have a considerably more complicated form [5], but retain the essential features of the Lagrange polynomials.

The total uncertainty is the quadrature sum of the calibration uncertainty $u_c(T)$, the uncertainty due to interpolation error, u_{18}, the uncertainty due to drift, $u_{19}(T)$, and the uncertainties occurring at the unknown temperature, $u_{20}(T)$:

$$u^2_{\text{total}}(T) = u^2_{\text{c}}(T) + u^2_{18} + u^2_{19}(T) + u^2_{20}(T). \quad (7)$$

The uncertainty component $u_{20}(T)$ accounts for the many contributions that occur when the thermometer is used, which, for reference thermometers measuring the temperature of blackbodies, includes many of the same u_1 to u_{17} components contributing to the calibration, but evaluated at the unknown temperature, T. Most of these must be treated separately according to the nature of the source and conditions during measurement. These uncertainty components each propagate according to

$$u_{20}(T) = \frac{\lambda_T T^2}{c_2} \left[1 - \exp\left(-c_2/\lambda_T T\right)\right] \frac{u_{20}(S)}{S}. \quad (8)$$

However, for some of the contributions there will exist strong correlations between the components during calibration and use, which will lead to partial or total cancellation of that term. The most obvious of these is non-linearity, which is almost entirely

a property of the thermometer and is not influenced by external conditions. A method for dealing with this sort of correlation is given in [10].

3 Uncertainty Components

In this section, each of the uncertainty components listed in Table 1 is briefly discussed. For more complete details, refer to [5]. Two different categories of uncertainty are referred to: "normal" and "best." Normal uncertainties refer to those easily obtained at present in national metrology institutes, and best uncertainties are those obtained with considerable effort by a small number of leading workers in the field. All uncertainties quoted in this article are standard uncertainties.

3.1 Uncertainties Associated with the Blackbody

3.1.1 Calibration Temperature

This contribution only applies to the VTBB scheme, where the blackbody temperature is measured by a separate reference thermometer. For best accuracy, a standard platinum resistance thermometer (SPRT) positioned near the bottom of the cavity and in good thermal contact with the heat transfer agent is used. For normal accuracy, the temperature measurement may be performed with a Pt100 (industrial platinum resistance thermometer with a resistance of 100 Ω at 0°C), a thermocouple, or any other secondary thermometer. The overall uncertainty of the temperature measurement stems from three groups of uncertainty contributions: the uncertainty of the calibration of the reference thermometer [11–13], the stability of the reference thermometer, and the uncertainty of the temperature measurement carried out by the user. Values of $u_1(T_i)$ range from 6 to 100 mK for normal accuracy and 0.8–3 mK for best accuracy, depending on the blackbody temperature.

3.1.2 Impurities

Impurities affect only the FPBB scheme. Metals of five nines (5N–99.999%) purity and six nines (6N–99.9999%) purity are commercially available from manufacturers. There are no definite indications of the effects on the fixed-point temperature of using purer samples than this, as the results are dependent on the nature and the distribution of the impurities inside the sample. The effect of impurities on the Zn point is discussed in [14]. A detailed experimental investigation of the effect of impurities on the Al point is reported in [15] and experimental investigations for the Ag and Cu points can be found in [16–18]. Differences of less than 10 mK have been found between 5N and 6N Ag samples. A detailed analysis with references on the influence of impurities can also be found in [13,19,20].

The effects of oxidation are important in radiation thermometry because of the use of open cells. A discussion of the oxidation effects for silver and aluminum FPBBs can be found in [21,22]. The effect of oxidation is not clear for zinc and other fixed-point metals with even lower transition temperatures. Indium is easily oxidized at its surface

and oxygen will penetrate inside the metal over time. Gallium also forms an oxidized surface layer. More research is required on the effect of metal oxidation.

Uncertainties due to impurities tend to increase with increasing transition temperature, so that $u_2(T_i)$ ranges from 0.75 to 6.5 mK for normal accuracy and 0.1–0.7 mK for best accuracy.

3.1.3 Plateau Identification

This contribution only applies to the FPBB scheme. If the freeze plateau is of good quality, the fixed-point temperature can be estimated, for example, as the average between 25% and 75% solid fraction of the freeze plateau. The difference between this average value and the maximum of the freezing curve is treated as the uncertainty in the fixed-point temperature. This uncertainty component should include the repeatability of the plateau assessed from multiple freeze plateaux, as well as any long-term drifts in the plateau due to possible degradation in furnace heaters, cavity wall surface conditions, etc. over an extended period of time. Values of $u_3(T_i)$ are 10 and 2 mK for the normal and best uncertainty, respectively, for all fixed points except for Ga and Hg, which have uncertainties up to 20 times higher due to the significant background radiation at low temperatures.

3.1.4 Blackbody Emissivity, Isothermal

The effective emissivity of both fixed-point and variable-temperature blackbody cavities may be determined either by calculation or measurement. Factors influencing the uncertainty in calculations of the effective emissivity include wall emissivity [23], geometry, machining imperfections, and the reflectance properties of the cavity surface [24–27]. A variety of mathematical models have been developed, mainly based on the summation method, the series method, or Monte Carlo simulations [28–30]. Experimental methods, based on reflectance measurements [31,32], generally result in slightly higher values than the calculated values, indicating that the emissivity estimates for the surfaces are slightly underestimated. These methods result in relative signal uncertainties, $u_4(S_i)/S_i$, of 0.0005 for normal accuracy and 0.000015 for best accuracy.

3.1.5 Blackbody Emissivity, Non-isothermal

For variable-temperature blackbodies that cannot be guaranteed to be isothermal, measurements of the temperature distribution along the walls of the cavity must be carried out [33,34] and the effective emissivity estimated based on a modified summation method [28] or a modified Monte Carlo simulation method [34]. For small departures from isothermal conditions, this results in a constant cavity temperature uncertainty, $u_5(T_i)$, of 35 mK for normal accuracy and 2.6 mK for best accuracy at all cavity temperatures and wavelengths.

3.1.6 Reflected Ambient Radiation

When viewing a blackbody, a small part of the radiation thermometer's signal arises from ambient radiation that enters the blackbody cavity's aperture and subsequently emerges after multiple reflections. The aperture can be treated as a diffuse reflector with a reflectance equal to $1 - \varepsilon_{bb}$, where ε_{bb} is the effective emissivity of the cavity. This reflection error is only significant for long wavelengths and low temperatures (near and below ambient). Correcting for reflections [35] results in uncertainties, $u_6(T_i)$, of up to 80 mK for normal accuracy and 13 mK for best accuracy. The effect is negligible for 0.9 and 1.6-μm thermometers. Note that this uncertainty contribution is highly correlated with the blackbody emissivity uncertainties.

3.1.7 Heat Loss Effects

The blackbody aperture is responsible for two heat loss effects – radiant heat exchange and convective heat loss. Radiant heat exchange produces a temperature gradient between the cavity bottom and the fixed-point metal (for the FPBB scheme) or the reference contact thermometer (for the VTBB scheme). Corrections for the heat loss can be applied [36,37], with the resulting uncertainty largely dominated by the uncertainty in the value assumed for the thermal conductivity of the cavity wall material, typically graphite. The thermal conductivity of graphite depends on many physical and chemical properties, so direct measurement at the appropriate temperature is the best approach. Extrapolation to different temperatures is also possible [38]. Uncertainties increase as the cavity temperature gets further from ambient, with values of $u_7(T_i)$ ranging up to 105 mK for normal accuracy and 35 mK for best accuracy.

Convection losses mainly affect large-aperture VTBBs and lead to a temperature deviation between the cavity radiance temperature and the reference thermometer. At sub-ambient temperatures, convection can also cause the formation of dew or ice on the cavity walls, increasing the temperature gradient and changing the cavity wall emissivity. The convection problem has been studied in detail in [23,39,40]. Values of $u_8(T_i)$ range up to 230 mK for normal accuracy and 12 mK for best accuracy.

3.1.8 Cavity Bottom Uniformity

Non-uniformity in the radiance temperature of a blackbody is only an issue in the VTBB scheme. The problem is worse for blackbodies with electric sheath heaters than for those using either fluid baths or heat pipes. The heat loss effects described above can also give rise to cavity bottom non-uniformities. The non-uniformity can be measured directly with a small-target radiation thermometer [39] or indirectly using reflectance techniques [41]. Values of $u_9(T_i)$ range from 30 to 100 mK for normal accuracy and 10–30 mK for best accuracy.

3.1.9 Ambient Conditions

The influence of ambient conditions on the uncertainty budget of a blackbody is identified with the noise of the radiance temperature of the blackbody, predominantly due

to the effects of feedback oscillations in the blackbody temperature control loop. For fixed-point blackbodies, this uncertainty is part of the uncertainty involved with the plateau identification, so this component only applies to the VTBB scheme. For large-aperture blackbodies, this noise can be measured with an SPRT positioned close to the bottom of the cavity and in good thermal contact with the heat-transfer agent. Values of $u_{10}(T_i)$ depend on the resolution of the temperature control loop and are estimated at 58 mK for normal accuracy and range from 5 to 12 mK for best accuracy [42].

3.2 Uncertainties Associated with the Radiation Thermometer

3.2.1 Size-of-Source Effect

For near-infrared thermometers (0.9 and 1.6 µm), the size-of-source effect (SSE) can be characterized in the same manner as for thermometers operating in the visible, using either the "direct" or "indirect" methods [43,44]. The SSE is found to be dependent on the design of the radiation thermometer [45], and whether a Lyot stop is present [46] or a simple single lens configuration is used [3]. However, in the mid- and thermal-infrared regions at low temperatures, background radiation at ambient temperature originating beyond the nominal source diameter can have a significant influence on the SSE signals. The SSE characterization must include the effects of this background radiation [47]. The relative signal uncertainty, $u_{11}(S_i)/S_i$, after correcting [5,48] for the SSE, is 0.0007 for normal accuracy and 0.000014 for best accuracy.

3.2.2 Non-linearity

Non-linearity is caused by the non-ideal performance of the detector, electronics, or both. Thus, if possible, measurements of non-linearity should be performed with the detector integrated into a system and not characterized separately. Non-linearity is commonly measured using "dual aperture" [49] or "superposition" [50] methods. Both methods sample the non-linearity at discrete points within the thermometer's temperature range. These points are used to derive a continuous non-linearity function with which corrections to measured signals can be made.

InGaAs detectors are commonly used at 1.6 µm, and these have been found to be non-linear with overfilling of the diode with radiation [51,52] and linear with underfilling [50,53]. For mid-infrared radiation thermometers centered at 3.9 µm, the ratio of Planck radiances can range from modest values, like $L(800°C)/L(157°C) = 176$, to demanding ratios, like $L(960°C)/L(20°C) = 15,500$, which is outside the range of linear behavior for radiation thermometers utilizing indium antimonide (InSb) detectors [54]. For the 8–14 µm thermal infrared radiation thermometer, the ratio of expected signals, $S(300°C)/S(-40°C) = 35$, is within the range of linear behavior for radiation thermometers utilizing mercury cadmium telluride (HgCdTe or MCT) detectors in the photovoltaic mode [55]. In contrast, a ratio $S(500°C)/S(-40°C) = 72$ is again outside the linear operation range.

Values of $u_{12}(S_i)/S_i$, after correction for non-linearity, tend to increase with increasing operating wavelength, and are in the range 0.0005–0.002 for normal accuracy and 0–0.0002 for best accuracy.

3.2.3 Effect of Instrument Temperature

The temperature of the thermometer itself affects the uncertainty budget through two different causes. Firstly, for target temperatures below about 200°C, the radiation produced by the detector is significant and must be taken into account [56]. The detected signal must be corrected through an internal measurement of some reference temperature, which may be the temperature of the detector or a reference cavity for chopped systems. The uncertainty in the reference temperature gives rise to uncertainties $u_{13}(T_i)$ at 10 µm of the order of 100 mK for normal accuracy and 10 mK for best accuracy. At 3.9 µm, these values are reduced by a factor of 20, while at 1.6 and 0.9 µm, the uncertainty is negligible.

Secondly, changes in thermometer temperature due to changes in ambient temperature or heating from the source affect the thermometer signal through changes in detector responsivity [57], temperature dependence of the amplifier, and shift in the filter wavelength. Controlling the temperature of these components minimizes the resulting uncertainty. At normal accuracy, $u_{14}(S_i)/S_i$ varies from 0.00008 to 0.0011, while at best accuracy, these uncertainties are 10 times smaller.

3.2.4 Atmospheric Absorption and Emission

In the infrared, absorption and emission of radiation by gas species in the atmosphere, particularly water vapor and carbon dioxide, can modify the signal detected by the thermometer. Absorption dominates if the blackbody source temperature is higher than ambient and emission dominates for lower source temperatures [58]. The magnitude of the error increases with both working distance and thermometer bandwidth. Application of a computed correction for these absorption and emission effects is rarely practical. However, because most thermometers operate over a relatively narrow bandwidth within an atmospheric window and working distances for calibration are seldom longer than 1 m, the absorption and emission effects are usually negligible [59]. Pessimistic values of $u_{15}(S_i)/S_i$, due to atmospheric effects, are estimated as 0.0003 for normal accuracy and 0.0001 for best accuracy.

3.2.5 Gain Ratios

Several different amplifier gains may be required to cover the operating temperature range for a particular thermometer. Knowledge of the gain ratios is necessary to normalize all signals to a common gain value before application of Eq. 2. Uncertainties arise from the measurement of the gain ratios and from possible temporal drift.

The thermometer signal changes by six orders of magnitude for a 1.6-µm thermometer within the range 150–960°C. For a 3.9-µm thermometer, the signal changes by four orders of magnitude between 20 and 960°C. For an 8–14-µm thermometer, the signal changes by less than two orders of magnitude from −40 to 500°C. Therefore,

Table 3 Uncertainty component, u_{18}, due to interpolation error (in mK) over the indicated temperature range for Planck and Wien versions of the Sakuma–Hattori equation (Eq. 2)

$\lambda = 0.9\,\mu m$, 400–1, 085°C		$\lambda = 1.6\,\mu m$, 150–960°C		$\lambda = 3.9\,\mu m$, 20–960°C		$\lambda = 10\,\mu m$, −40–500°C	
Wien	Planck	Wien	Planck	Wien	Planck	Wien	Planck
1.6	1.5	4.9	3.6	740	1.0	870	15

different gains are not required for the 8–14-μm thermometer, and it is only the short-term stability of the gain that leads to uncertainty in this case. Values of $u_{16}(S_i)/S_i$ vary from 1×10^{-5} to 1×10^{-4} for normal accuracy, and from 2×10^{-6} to 1×10^{-5} for best accuracy.

3.2.6 Noise

The contribution of noise to the uncertainty can become considerable when measuring close to the lower limit of the instrument's measurement temperature range, although this increase in noise at lower temperatures is usually compensated somewhat by a decrease in electrical bandwidth. Also, the signal can become noisy due to quantization error. It is important when sampling the noise contribution to ensure than none of the effects discussed above is included, otherwise "double-counting" will occur. Sources of noise in detectors are discussed in [60]. Values of $u_{17}(T_i)$ range from 10 to 75 mK at normal accuracy and from 2 to 25 mK at best accuracy.

3.3 Interpolation Error

Interpolation error describes the difference between the temperature determined using Eq. 2 and the temperature that would be calculated from Eq. 1 if the relative spectral responsivity were known. In [61], it is shown that this interpolation error has the form of a third-order polynomial in T, with zeros at T_1, T_2, and T_3 when $N = 3$, and zeros at three other points within the calibration range when $N > 3$. The amplitude of the polynomial is a function of the operating wavelength and bandwidth of the thermometer and is proportional to the cube of the calibration temperature range. Table 3 gives the uncertainty due to interpolation error for both the Planck and Wien versions of Eq. 2, where the uncertainty is determined by treating the amplitude of the interpolation error as the limits of a rectangular distribution. For the 3.9 and 10-μm thermometers, there is a clear advantage in using the Planck version of the Sakuma–Hattori equation.

3.4 Drift

Drift in radiation thermometers between calibrations arises from changes in the optical components, the radiation detector, and the electronics measuring the detector signal.

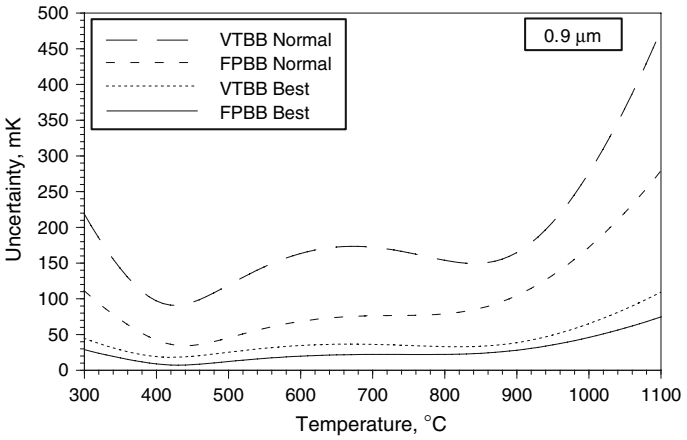

Fig. 1 Total uncertainty (excluding drift) for a 0.9-µm thermometer using three calibration points. For the FPBB scheme, the calibration points are the Zn, Al, and Ag points, and for the VTBB scheme, they are 400, 700, and 960°C

Drift has the effect of modifying some or all the A, B, and C parameters of Eq. 2 [62]. If the drift is too large, it can be eliminated by re-determining the A, B, and C parameters using new calibration data.

Away from their band edge, semiconductor detectors are generally extremely stable, with drifts of typically $0.1\% \cdot \mathrm{yr}^{-1}$ and as low as $0.02\% \cdot \mathrm{yr}^{-1}$ [63]. Near to the band edge, the response generally becomes both very temperature sensitive and much more unstable. Pyroelectric detectors are less stable than photodiodes, with typical stability of $0.2\% \cdot \mathrm{yr}^{-1}$.

Drifts due to the optical components can be divided into shifts in transmission in the bandpass of the radiation thermometer and shifts in the effective wavelength. With proper care, window and lens transmission can be stable to better than 0.05%, although cleaning, etc. can change the transmission by up to a few tenths of a percent. For 10 µm devices, mirror optics are generally used, which have poorer stability than refractive components, typically about $0.5\% \cdot \mathrm{yr}^{-1}$ [63].

Multilayer interference filters are more unstable than windows and lenses, typically decreasing the signal by about $0.2\% \cdot \mathrm{yr}^{-1}$. They also exhibit a type of secular drift arising from the internal stresses generated during deposition, which slowly anneal. This causes a drift in the mean wavelength of the filter, proportional to the wavelength, e.g., $0.1\,\mathrm{nm} \cdot \mathrm{yr}^{-1}$ at 650 nm, but $0.3\,\mathrm{nm} \cdot \mathrm{yr}^{-1}$ at 1600 nm, etc. [63]. The effects of drift lead to values of the uncertainty $u_{19}(T)$ in the range from 250 to 500 mK at normal accuracy and from 80 to 250 mK at best accuracy over a period of one year.

4 Combined Uncertainties

Equation 7 gives the total combined uncertainty (in the absence of correlations) in the calibration and subsequent use of a radiation thermometer using the interpolation

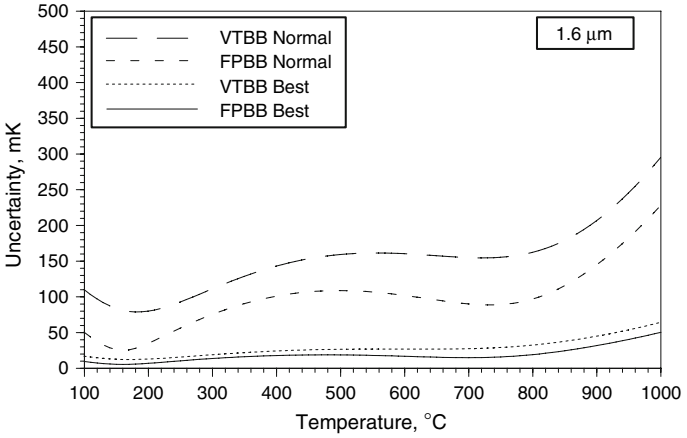

Fig. 2 Total uncertainty (excluding drift) for a 1.6-µm thermometer using three calibration points. For the FPBB scheme, the calibration points are the In, Al, and Ag points, and for the VTBB scheme, they are 150, 550, and 960°C

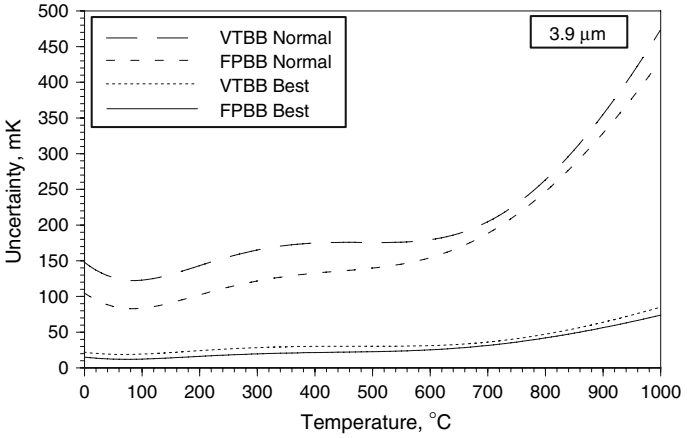

Fig. 3 Total uncertainty (excluding drift) for a 3.9-µm thermometer using three calibration points. For the FPBB scheme, the calibration points are the Ga, Zn, and Ag points, and for the VTBB scheme, they are 20, 470, and 960°C

technique. The options for operating wavelength and calibration points are too numerous to tabulate individually, so in this section some representative examples only are plotted. The details presented in [5] allow calculations to be carried out for other conditions.

Figures 1–4 plot the calibration uncertainty for 0.9, 1.6, 3.9, and 10 µm thermometers, respectively, for both the FPBB scheme and VTBB scheme for normal and best accuracy. These curves do not include the drift component, $u_{19}(T)$, or any of the in-use components, $u_{20}(T)$, other than the non-linearity component, which is strongly

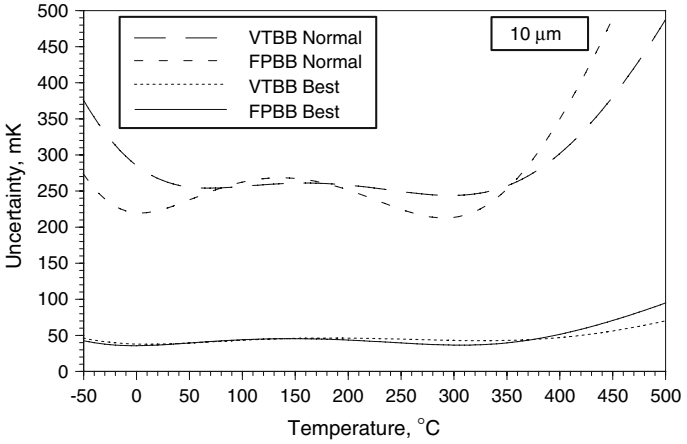

Fig. 4 Total uncertainty (excluding drift) for an 8–14-µm thermometer using three calibration points. For the FPBB scheme, the calibration points are the Hg, Sn, and Zn points, and for the VTBB scheme, they are −40, 230, and 500°C

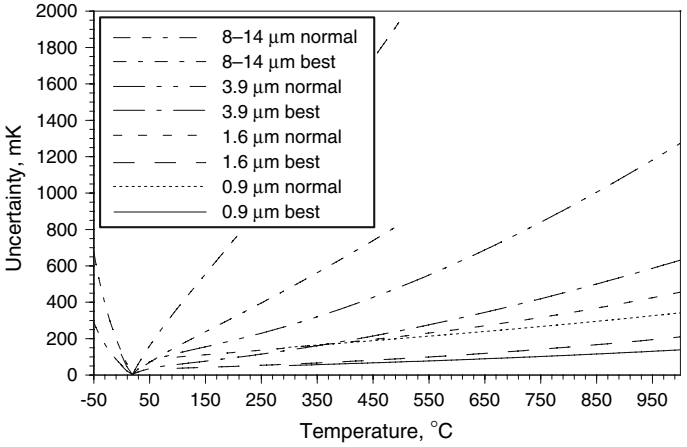

Fig. 5 Component of uncertainty due to drift over one year

correlated with the non-linearity components during measurements at the calibration points. Each curve corresponds to three calibration temperatures as indicated in the figure captions. The drift component over one year is plotted separately in Fig. 5 for each thermometer and the sensitivity coefficients for the in-use components (expressed as mK per percent signal uncertainty at the unknown temperature) are plotted in Fig. 6. The total uncertainty for a temperature measurement is obtained from the quadrature sum of the appropriate curve in Figs. 1–4, a fraction of Fig. 5, and Fig. 6 multiplied by the in-use percentage signal uncertainty at the measured temperature.

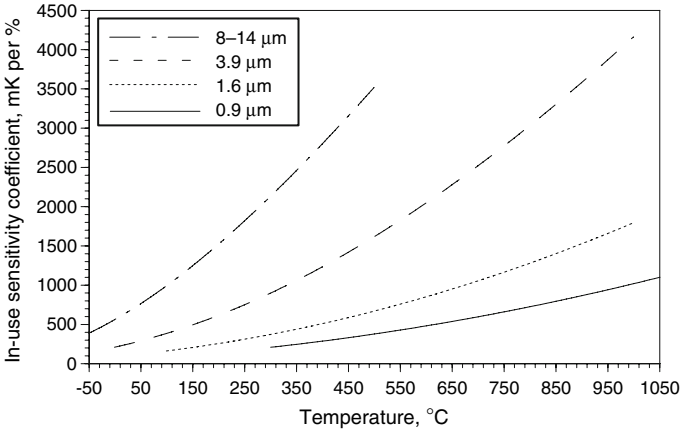

Fig. 6 Sensitivity coefficients for the in-use components of uncertainty expressed as mK per percent uncertainty in the thermometer signal

Acknowledgment The authors would like to thank Mr. Yoshiro Yamada of NMIJ for his valuable input to the content of the original uncertainty guide [5].

References

1. P. Saunders, Metrologia **34**, 201 (1997)
2. F. Sakuma, M. Kobayashi, in *Proceedings of TEMPMEKO '96, 6th International Symposium on Temperature and Thermal Measurements in Industry and Science*, ed. by P. Marcarino (Levrotto and Bella, Torino, 1997), pp. 305–310
3. B. Gutschwager, J. Fischer, in *Proceedings of TEMPMEKO '99, 7th International Symposium on Temperature and Thermal Measurements in Industry and Science*, ed. by J.F. Dubbeldam, M.J. de Groot (Edauw Johannissen bv, Delft, 1999), pp. 567–572
4. F. Sakuma, S. Hattori, in *Temperature: Its Measurement and Control in Science and Industry*, vol. 5, ed. by J.F. Schooley (AIP, New York, 1982), pp. 421–427
5. J. Fischer, P. Saunders, M. Sadli, M. Battuello, C.W. Park, Z. Yuan, H. Yoon, W. Li, E. van der Ham, F. Sakuma, Y. Yamada, M. Ballico, G. Machin, N. Fox, J. Hollandt, M. Matveyev, P. Bloembergen, S. Ugur, CCT working document (in preparation)
6. J. Fischer, M. Battuello, M. Sadli, M. Ballico, S.N. Park, P. Saunders, Z. Yuan, B.C. Johnson, E. van der Ham, W. Li, F. Sakuma, G. Machin, N. Fox, S. Ugur, M. Matveyev, CCT document CCT/03-03 (2003)
7. J. Fischer, M. Battuello, M. Sadli, M. Ballico, S.N. Park, P. Saunders, Z. Yuan, B.C. Johnson, E. van der Ham, F. Sakuma, G. Machin, N. Fox, W. Li, S. Ugur, M. Matveyev, in *Temperature: Its Measurement and Control in Science and Industry*, vol. 7, ed. by D.C. Ripple, B.C. Johnson, C.W. Meyer, R.D. Saunders, G.F. Strouse, W.L. Tew, B.K. Tsai, H.W. Yoon (AIP, Melville, New York, 2003), pp. 631–638
8. *Guide to the Expression of Uncertainty in Measurement* (International Organization for Standardization, Geneva, 1993)
9. P. Saunders, Metrologia **40**, 93 (2003)
10. P. Saunders, D.R. White, in *Proceedings of TEMPMEKO 2007*, Int. J. Thermophys. **28**, 2098 (2007), doi: 10.1007/s10765-007-0244-5
11. E. Renaot, G. Bonnier, CCT document CCT/2000-16 (2000)
12. E. Renaot, G. Bonnier, CCT document CCT/2000-17 (2000)
13. B. Fellmuth, J. Fischer, E. Tegeler, CCT document CCT/01-02 (2001)

14. J. Wu, Z. Yuan, Y. Duan, T. Wang, Q. Zhao, in *Proceedings of TEMPMEKO 2001, 8th International Symposium on Temperature and Thermal Measurements in Industry and Science*, ed. by B. Fellmuth, J. Seidel, G. Scholz (VDE Verlag, Berlin, 2002), pp. 189–194
15. J. Ancsin, Metrologia **40**, 36 (2003)
16. G. Bongiovanni, L. Crovini, P. Marcarino, Metrologia **11**, 125 (1975)
17. T. Ricolfi, F. Lanza, High Temp. High Press. **9**, 483 (1977)
18. J. Fischer , H.J. Jung, Metrologia **26**, 245 (1989)
19. B.W. Mangum, P. Bloembergen, B. Fellmuth, P. Marcarino, A.I. Pokhodun, CCT Document CCT/99-11 (1999)
20. D. Ripple, B. Fellmuth, M. de Groot, Y. Hermier, K.D. Hill, P.P.M. Steur, A. Pokhodun, M. Matveyev, P. Bloembergen, CCT WG1 report, CCT Document CCT/05-08 (2005)
21. H. Okamoto, *Desk Handbook: Phase Diagrams for Binary Alloys* (ASM International, Materials Park, Ohio, 2000), p. 14
22. L. Ma, F. Sakuma, in *Proc. SICE2004* (Sapporo, Japan, 2004), pp. 323–328
23. E.W.M. van der Ham, M. Battuello, P. Bloembergen, R. Bosma, S. Clausen, O. Enouf, E. Filipe, J. Fischer, B. Gutschwager, T. Hirvonen, J.U. Holtoug, J. Ivarson, G. Machin, H. McEvoy, J. Peres, T. Ricolfi, P. Ridoux, M. Sadli, V. Schmidt, C. Staniewicz, O. Struss, T. Weckstrom, F. Girard, TRIRAT: Traceability in infrared radiation thermometry from −50 to 800°C. Framework 4 Project of the Standards, Measurement and Testing Programme of the European Commission, Contract No. SMT 4-CT-96-2060
24. Y. Shimizu, J. Ishii, F. Sakuma, A. Ono, in *Proceedings of TEMPMEKO 2004, 9th International Symposium on Temperature and Thermal Measurements in Industry and Science*, ed. by D. Zvizdić, L.G. Bermanec, T. Veliki, T. Stašić (FSB/LPM, Zagreb, Croatia, 2004), pp. 509–514
25. T.P. Jones, in *Temperature: Its Measurement and Control in Science and Industry*, vol. 6, ed. by J.F. Schooley (AIP, New York, 1992), pp. 1105–1110
26. M. Ballico, Metrologia **32**, 259 (1995/6)
27. S. Mekhontsev, V. Khromchenko, A. Prokhorov, L. Hanssen, in *Proceedings of TEMPMEKO 2004, 9th International Symposium on Temperature and Thermal Measurements in Industry and Science*, ed. by D. Zvizdić, L.G. Bermanec, T. Veliki, T. Stašić (FSB/LPM, Zagreb, Croatia, 2004), pp. 581–586
28. R.E. Bedford, in *Theory and Practice of Radiation Thermometry*, ed. by D.P. DeWitt, G.D. Nutter (John Wiley & Sons, New York, 1988)
29. V.I. Sapritsky, A.V. Prokhorov, Metrologia **29**, 9 (1992)
30. J. Ishii, M. Kobayashi, F. Sakuma, Metrologia **35**, 175 (1998)
31. M. Ballico, Metrologia **37**, 295 (2000)
32. M. Ballico, in *Proceedings of TEMPMEKO 2004, 9th International Symposium on Temperature and Thermal Measurements in Industry and Science*, ed. by D. Zvizdić, L.G. Bermanec, T. Veliki, T. Stašić (FSB/LPM, Zagreb, Croatia, 2004), pp. 841–846
33. J. Hartmann, D. Taubert, J. Fischer, in *Proceedings of TEMPMEKO '99, 7th International Symposium on Temperature and Thermal Measurements in Industry and Science*, ed. by J.F. Dubbeldam, M.J. de Groot (Edauw Johannissen bv, Delft, 1999), pp. 511–516
34. J. Hartmann, S. Schiller, R. Friedrich, J. Fischer, in *Proceedings of TEMPMEKO 2001, 8th International Symposium on Temperature and Thermal Measurements in Industry and Science*, ed. by B. Fellmuth, J. Seidel, G. Scholz (VDE Verlag, Berlin, 2002), pp. 227–232
35. P. Saunders, *Radiation Thermometry: Fundamentals and Applications in the Petrochemical Industry* (SPIE Press, Bellingham, Washington, 2007)
36. H.J. Jung, Inst. Phys. Conf. Ser. No. 26, p. 278 (1975)
37. P. Jimeno-Largo, Y. Yamada, P. Bloembergen, M.A. Villamanan, G. Machin, in *Proceedings of TEMPMEKO 2004, 9th International Symposium on Temperature and Thermal Measurements in Industry and Science*, ed. by D. Zvizdić, L.G. Bermanec, T. Veliki, T. Stašić (FSB/LPM, Zagreb, Croatia, 2004), pp. 335–340
38. H. McEvoy, G. Machin, *Report on the thermal conductivity of graphite*, produced for CCT WG5 (2001)
39. J. Fischer, in *Proceedings of TEMPMEKO '99, 7th International Symposium on Temperature and Thermal Measurements in Industry and Science*, ed. by J.F. Dubbeldam, M.J. de Groot (Edauw Johannissen bv, Delft, 1999), pp. 27–34

40. J. Ishii, A. Ono, in *Temperature: Its Measurement and Control in Science and Industry*, vol. 7, ed. by D.C. Ripple, B.C. Johnson, C.W. Meyer, R.D. Saunders, G.F. Strouse, W.L. Tew, B.K. Tsai, H.W. Yoon (AIP, Melville, New York, 2003), pp. 657–662
41. M. Ballico, in *Proceedings of TEMPMEKO 2001, 8th International Symposium on Temperature and Thermal Measurements in Industry and Science*, ed. by B. Fellmuth, J. Seidel, G. Scholz (VDE Verlag, Berlin, 2002), pp. 233–237
42. J. Hollandt, Private communication
43. D. Lowe, M. Battuello, G. Machin, F. Girard, in *Temperature: Its Measurement and Control in Science and Industry*, vol. 7, ed. by D.C. Ripple, B.C. Johnson, C.W. Meyer, R.D. Saunders, G.F. Strouse, W.L. Tew, B.K. Tsai, H.W. Yoon (AIP, Melville, New York, 2003), pp. 625–630
44. G. Machin, R. Sergienko, in *Proceedings of TEMPMEKO 2001, 8th International Symposium on Temperature and Thermal Measurements in Industry and Science*, ed. by B. Fellmuth, J. Seidel, G. Scholz (VDE Verlag, Berlin, 2002), pp. 155–160
45. H.W. Yoon, D.W. Allen, R.D. Saunders, Metrologia **42**, 89 (2005)
46. T. Ricolfi, F. Girard, in *Proceedings of TEMPMEKO '99, 7th International Symposium on Temperature and Thermal Measurements in Industry and Science*, ed. by J.F. Dubbeldam, M.J. de Groot (Edauw Johannissen bv, Delft, 1999), pp. 593–598
47. P. Bloembergen, in *Proceedings of TEMPMEKO '99, 7th International Symposium on Temperature and Thermal Measurements in Industry and Science*, ed. by J.F. Dubbeldam, M.J. de Groot (Edauw Johannissen bv, Delft, 1999), pp. 607–612
48. P. Bloembergen, Y. Duan, R. Bosma, Z. Yuan, in *Proceedings of TEMPMEKO '96, 6th International Symposium on Temperature and Thermal Measurements in Industry and Science*, ed. by P. Marcarino (Levrotto and Bella, Torino, 1997), pp. 261–266
49. K.D. Mielenz, K.L. Eckerle, Appl. Optics **11**, 2294 (1972)
50. H.W. Yoon, J.J. Butler, T.C. Larason, G.P. Eppeldauer, Metrologia **40**, S154 (2003)
51. L.P. Boivin, Metrologia **37**, 273 (2000)
52. P. Corredera, M.L. Hernanz, M. González-Herráez, J. Campos, Metrologia **40**, S150 (2003)
53. M. Battuello, P. Bloembergen, F. Girard, T. Ricolfi, in *Temperature: Its Measurement and Control in Science and Industry*, vol. 7, ed. by D.C. Ripple, B.C. Johnson, C.W. Meyer, R.D. Saunders, G.F. Strouse, W.L. Tew, B.K. Tsai, H.W. Yoon (AIP, Melville, New York, 2003), pp. 613–618
54. L.P. Boivin, Appl. Optics **37**, 1924 (1998)
55. E. Theocharous, J. Ishii, N.P. Fox, Appl. Optics **43**, 4182 (2004)
56. J. Ishii, M. Kobayashi, F. Sakuma, A. Ono, in *Proceedings of TEMPMEKO '99, 7th International Symposium on Temperature and Thermal Measurements in Industry and Science*, ed. by J. F. Dubbeldam, M.J. de Groot (Edauw Johannissen bv, Delft, 1999), pp. 625–630
57. O. Struβ, in *Temperature: Its Measurement and Control in Science and Industry*, vol. 7, ed. by D.C. Ripple, B.C. Johnson, C.W. Meyer, R.D. Saunders, G.F. Strouse, W.L. Tew, B.K. Tsai, H.W. Yoon (AIP, Melville, New York, 2003), pp. 565–570
58. P. Saunders, in *Temperature: Its Measurement and Control in Science and Industry*, vol. 7, ed. by D.C. Ripple, B.C. Johnson, C.W. Meyer, R.D. Saunders, G.F. Strouse, W.L. Tew, B.K. Tsai, H.W. Yoon (AIP, Melville, New York, 2003), pp. 825–830
59. K. Chrzanowski, Appl. Optics **35**, 3540 (1996)
60. D.G. Crowe, P.R. Norton, T. Limperis, J. Mudar, Chapter 4 "Detectors", in *The Infrared and Electro-Optical Systems Handbook*, *Electro-Optical Components*, vol. 3, ed. by W. D. Rogatto (SPIE Optical Engineering Press, Bellingham, Washington, 1993)
61. P. Saunders, D.R. White, Metrologia **41**, 41 (2004)
62. P. Saunders, D.R. White, Metrologia **40**, 195 (2003)
63. M. Ballico, Private communication